Relating structural, magnetic-moment, and hyperfine-field behavior to a local-environment model in $Fe_{3-x}Co_xSi$

V. Niculescu,* J. I. Budnick, W. A. Hines, and K. Raj†
Department of Physics and Institute of Materials Science, University of Connecticut, Storrs, Connecticut 06268

S. Pickart
Department of Physics, University of Rhode Island, Kingston, Rhode Island 02881

S. Skalski
Department of Physics, Fordham University, Bronx, New York 10458
(Received 12 June 1978)

A detailed NMR, magnetization, x-ray, and neutron-diffraction study is reported for the $Fe_{3-x}Co_xSi$ system over the entire range of Co concentration ($0 \leq x \leq 3.00$). As the Co concentration x is increased, the x-ray measurements indicate that a single phase having the fcc DO_3-type structure is maintained (with some variation in lattice constant) up to $x = 2.15$. It is found that Co selectively enters the (A,C) sites for the higher concentrations studied in this work ($x \leq 2.00$) with a high degree of order for $x < 1.50$. The variation in lattice constant with Co concentration correlates well with the bulk magnetization and can be described by a simple empirical relation which is an extension of Vegard's law. Neutron-diffraction and magnetization measurements have enabled a determination of the Fe(B), Fe(A,C), and Co(A,C) magnetic-moment dependence on Co concentration for these alloys. In particular, we note that the moment on the substituted Co atoms appears well localized and remains essentially constant ($+1.7\mu_B$) throughout the range $0 \leq x \leq 2.15$. In addition, the variations of the internal hyperfine fields with Co concentration at all sites [Fe(B), Fe(A,C), Co(A,C), and Si(D)] have been studied by spin-echo NMR. In order to explain the magnetic-moment and internal field behavior, a model emphasizing the short range interaction approach is presented. Since Co enters the (A,C) sites, the short range interaction model involves only the $1nn$ configurations for the Fe(B) atoms. The model successfully describes the detailed behavior of the magnetic moments and internal fields at all sites and enables a subdivision of the observed internal field into contributions due to the $4s$ spin polarization transferred from neighboring moments and the polarization resulting from the on-site moment. Such an approach has already proved successful for transition metal substitutions into the B sites.

I. INTRODUCTION

Recently, a great deal of attention has been focused on the ferromagnetic intermetallic compound Fe_3Si and its related ternary alloys of the form $Fe_{3-x}T_xSi$, where T is a transition-metal element.[1-17] The existence of a unique preferential site-substitution pattern, along with almost perfect atomic ordering, provides opportunities for correlating magnetic-moment formation and hyperfine-field interactions with local environment configurations. This paper concerns the application of NMR, bulk magnetization, x-ray, and neutron-diffraction techniques in such a study of the $Fe_{3-x}Co_xSi$ system throughout the entire range of composition ($0 \leq x \leq 3.00$).

Fe_3Si is a crystallographically well-ordered ferromagnet with a Curie temperature of 839 K.[1,2,18] It possesses a fcc DO_3-type structure with four crystal sites A, B, C, and D and a crystallographic ordering temperature of 1378 K (see Fig. 1).[19] A tabulation of the number and type of first, second, etc., nearest neighbors (nn) for the ordered structure is provided in Table I. The Fe atoms are located in three of the crystal sites A, B, and C, with A and C being chemically and magnetically equivalent. Fe atoms in the A and C sites, denoted by Fe(A, C), have four Fe(B)

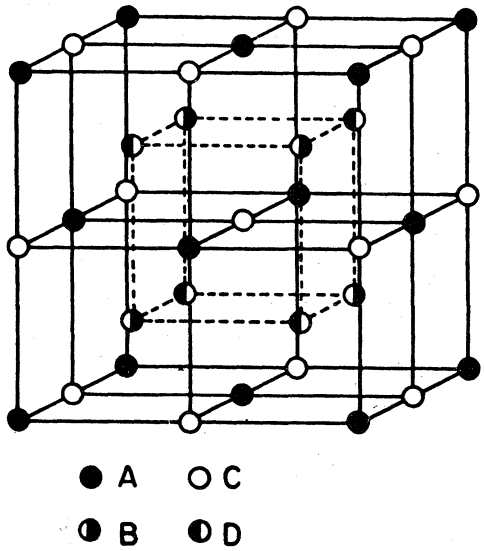

FIG. 1. Unit cell for Fe_3Si. The sites are represented by A,B,C, and D. The A and C sites are equivalent and are occupied by Fe atoms, the B sites are occupied by Fe atoms, and the D sites by Si atoms.

TABLE I. Nearest-neighbor arrangement for ordered Fe_3Si.

No. of shell	1	2	3	4	5	6	7	8
Neighbor distance in lattice parameters	0.43	0.5	0.705	0.83	0.86	1	1.08	1.11
		6*A*, *C*	12*A*, *C*		8*A*, *C*	6*A*, *C*		24*A*, *C*
A, *C*	4*B*			12*B*			12*B*	
	4*D*			12*D*			12*D*	
	8*A*, *C*			24*A*, *C*			24*A*, *C*	
B			12*B*			6*B*		
		6*D*			8*D*			24*D*
	8*A*, *C*			24*A*, *C*			24*A*, *C*	
D		6*B*			8*B*			24*B*
			12*D*			6*D*		

and four Si(*D*) as first-nearest neighbors (1nn) and carry a moment of $+1.35\mu_B$, while the Fe(*B*) have eight Fe(*A*, *C*) 1nn and carry a moment of $+2.20\mu_B$.[3] The Si(*D*) also have eight Fe(*A*, *C*) 1nn, however, they carry only a small moment of $-0.07\mu_B$.[3]

It has been demonstrated by NMR,[4,5] and subsequently confirmed by neutron-diffraction[6,7] and Mössbauer experiments,[8] that when transition-metal impurities are added to Fe_3Si, those elements to the right and below Fe in the periodic table substitute into the (*A*, *C*) sites while those elements to the left of Fe in the periodic table substitute into the *B* sites. A theoretical basis for this site preference based on rigid-band calculations has been provided by Switendick.[9,10]

The original NMR work cited above, which established the site selection pattern, was carried out on several $Fe_{3-x}T_xSi$ alloys consisting of dilute concentrations ($x \leq 0.25$) of transition-metal elements *T* from the 3*d*, 4*d*, and 5*d* series.[5] A detailed study of the saturation magnetization was subsequently made for dilute concentrations ($x \leq 0.25$) of the $Fe_{3-x}T_xSi$ system, where *T* = Ti, V, Cr, Mn, Co, and Ni.[3] The results were discussed in terms of moment assignments for the various substituted elements and disturbances of neighboring Fe moments. The nature of the site selectivity was further explored in the $Fe_{3-x}Mn_xSi$ system over a wide range of composition, $0 \leq x \leq 1.60$.[11] NMR and x-ray measurements resulted in a direct correlation of the magnetic structure and internal hyperfine-field values with the degree of local atomic ordering. Recently, x-ray, magnetization, and NMR techniques were used to determine the atomic ordering along with the variations in the local moments and internal field distributions in the $Fe_{3-x}V_xSi$ system over the composition range $0 \leq x \leq 1.25$.[1] In that work, a short-range interaction model was proposed which described the dependence of the Fe(*A*, *C*) moments on their 1nn configurations and enabled an evaluation of the role of the transferred conduction-electron-spin polarization in the hyperfine interaction picture for both the $Fe_{3-x}Mn_xSi$ and $Fe_{3-x}V_xSi$ systems.

In the studies described above, both Mn and V are to the left of Fe in the periodic table and enter the *B* sites. Until now, no such systematic study over a wide range of composition has been made on a $Fe_{3-x}T_xSi$ system in which the *T* element substitutes into the (*A*, *C*) sites. Such a study is of particular interest because both 2nn and 3nn *T*-*T* configurations are important for the (*A*, *C*) site substitution, while only the 3nn *T*-*T* configurations are important for the *B*-site substitution described above (see Table I). Consequently, the present investigation on $Fe_{3-x}Co_xSi$ over the entire range of composition ($0 \leq x \leq 3.00$) was initiated. In this paper, we report a detailed NMR, magnetization, x-ray, and neutron-diffraction study which enables us to (i) obtain valuable information concerning the crystallographic and magnetic structure of this system, (ii) further explore the nature of the selective site mechanism and determine the concentration limits of the selectively, and (iii) determine directly the dependences of the Fe, Co, and Si magnetic moments and internal fields on the local environment. Also, a model based on the short-range interaction approach and involving 1nn configurations for the Fe(*B*) atoms is presented. The model successfully describes the detailed behavior of the magnetic moments and internal fields at all sites and enables a subdivision of the observed field into contributions due to the polarization transferred from neighboring moments and the polarizations resulting from the on-site moment.

II. EXPERIMENTAL PROCEDURE AND RESULTS

A. Sample preparation

Pure Fe (99.999%), Co (99.999%), and Si (99.99%) were mixed in the appropriate propor-

tions to make 10-g ingots of the $Fe_{3-x}Co_xSi$ alloys with the following compositions: $x = 0$, 0.04, 0.08, 0.15, 0.25, 0.50, 0.75, 0.90, 1.00, 1.25, 1.50, 1.75, 2.00, 2.15, 2.25, 2.50, and 3.00. The constituents were melted together several times in an argon arc furnace to ensure homogeneity. The weight loss after arc melting was typically less than 1% for all the alloys. The resulting 10-g ingots were sealed under vacuum (2×10^{-6} Torr) in quartz tubes and homogenized for 40 h at 850 °C. The temperature was reduced slowly over a period of 4 h to 600 °C, maintained at 600 °C for an additional hour and subsequently quenched into room-temperature water. The ingots were powdered to No. 325 mesh size in a mortar and pestle. (It was found that the samples became progressively harder to grind with increasing Co content x.) The powders were annealed in a quartz tube under vacuum (2×10^{-6} Torr) for 1 h at 600 °C and subsequently allowed to cool naturally to room temperature.

The above heat treatment was selected because of previous success in preparing well-ordered Fe_3Si and the ternary systems $Fe_{3-x}V_xSi$ and $Fe_{3-x}Mn_xSi$.[1,3,11] As indicated below, all of the $Fe_{3-x}Co_xSi$ alloys studied in this work demonstrated a high degree of crystallographic order with this heat treatment.

B. X-ray diffraction

X-ray measurements were made at room temperature on the $Fe_{3-x}Co_xSi$ alloys with a Philips diffractometer using Cu $K\alpha$ radiation. For compositions up to and including $x = 2.15$, the samples were single phase and the x-ray diffraction pattern could be indexed on a fcc structure. Lattice parameters were determined by extrapolating the parameters corresponding to reflections from the (440), (620), and (444) planes to $\theta = 90°$ for both $K\alpha_1$ and $K\alpha_2$ radiation. Figure 2 shows the variation of the room-temperature lattice constant for the $Fe_{3-x}Co_xSi$ alloys with Co concentration x. The closed circles are the values obtained from x-ray measurements while the dashed curve represents a fit to the data based on an extension of Vegard' s law (see Sec. III A).

For this structure, Bragg reflections are produced by either all even or all odd Miller indices (h, k, l). As described in detail elsewhere, observation of the various x-ray line intensities provides information concerning the state of chemical order.[1,11] The reflections for which h, k, l are all even with $\frac{1}{2}(h+k+l) = 2n$, n being an integer, are fundamental and unaffected by the state of order. Those reflections for which h, k, l are all even with $\frac{1}{2}(h+k+l) = 2n+1$ or h, k, l are all odd are superlattice reflections with intensities depending on the state of order. When a random disorder occurs in ternary alloys of this type, all the superlattice lines are reduced in intensity by the same factor. However, if preferential disorder occurs between certain sites, certain groups of superlattice reflections will be affected differently and, generally, it is necessary to have more than one parameter for the characterization of the state of order. In particular, the intensities of the (111) and (200) superlattice lines have been measured in relation to the (444) fundamental line in order to provide a qualitative measure of the state of order for the various $Fe_{3-x}Co_xSi$ alloys.

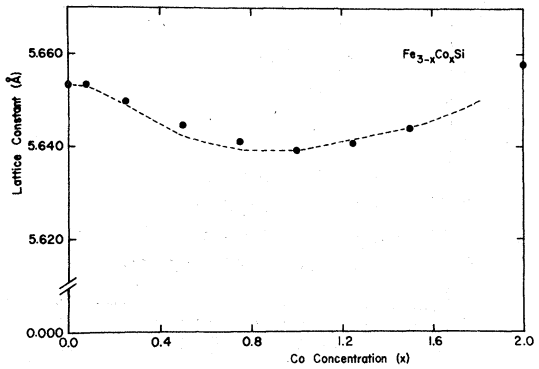

FIG. 2. Lattice constant a (in Å) vs Co concentration x, for $Fe_{3-x}Co_xSi$ at room temperature. Closed circles: experimental data; dashed curve: empirical relation involving an extension of Vegard's law.

Measurements on a Fe_3Si sample that was carefully prepared by the procedure described above in Sec. II A showed essentially no disorder between Fe and Si sites ($\lesssim 3\%$). In the $Fe_{3-x}Co_xSi$ system, previous NMR, neutron-diffraction, and Mössbauer investigations have demonstrated that small amounts of Co substitute for Fe in the (A,C) sites.[4-6,8] In general, for this system $B \rightarrow D$, $(A,C) \rightarrow B$, and $(A,C) \rightarrow D$ disorder can occur. Since Fe ($Z = 26$) and Co ($Z = 27$) are very close to each other in the periodic table, their x-ray scattering factors are similar and thus disorder between the (A,C) and B sites cannot be detected by x-ray measurements. However, the neutron scattering amplitudes for Co and Fe are quite different (0.25×10^{-12} and 0.96×10^{-12} cm, respectively) making possible the detection of any such disorder by neutron diffraction. In contrast to $(A,C) \rightarrow B$ disorder, the $B \rightarrow D$ and $(A,C) \rightarrow D$ disorder can be detected by the x-ray methods described above. In Fig. 3 we show the variation of the $B \rightarrow D$, $(A,C) \rightarrow B$, and $(A,C) \rightarrow D$ disorder as a function of x for the $Fe_{3-x}Co_xSi$ alloys. The various disorder values which were obtained from x-ray diffraction, neutron diffraction, and NMR are indicated. The four $(A,C) \rightarrow B$ disorder values obtained for

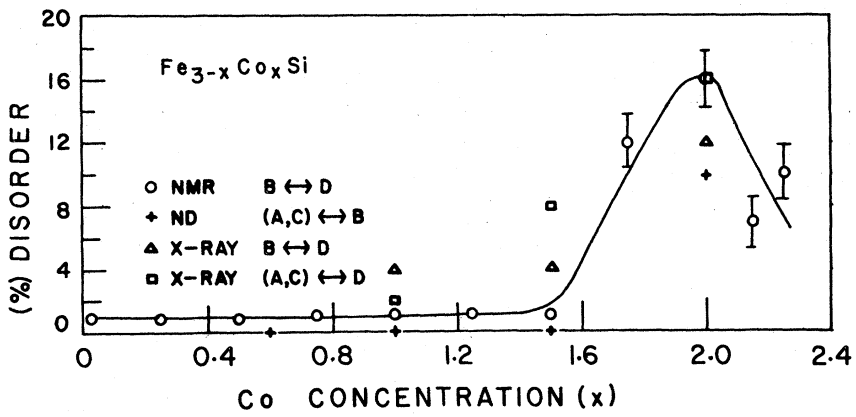

FIG. 3. Variation of the $(A,C) \leftrightarrow B$, $(A,C) \leftrightarrow D$, and $B \leftrightarrow D$ disorders vs Co concentration x, for $Fe_{3-x}Co_xSi$. The values obtained from x-ray (triangles and squares), neutron diffraction (crosses), and NMR (circles) are indicated.

$x = 0.50$, 1.00, 1.50, and 2.00 (crosses) are directly measured by neutron diffraction (see Sec. II D). The $(A,C) \leftrightarrow D$ (squares) and $B \leftrightarrow D$ (triangles) disorder values are calculated from x-ray differaction intensities with the assumption that the $(A,C) \leftrightarrow B$ disorder is small for $0 \leq x \leq 1.50$. The $B \leftrightarrow D$ disorder values (circles) obtained from NMR measurements will be discussed in Sec. II E.

C. Bulk magnetization

All measurements of the bulk magnetization σ and magnetic ordering temperature T_c were carried out on a PAR model 155 vibrating sample magnetometer (Foner method[20]). Temperatures ranging continuously from 3 to 1050 K were obtained with the related cryogenic and oven accessories while magnetic fields were available up to 20 kOe. The magnetometer was calibrated against the known saturation magnetization for Ni (room-temperature value of 55.01 emu/g. The temperature calibration below room temperature was based on the ideal Curie-Weiss behavior of the paramagnetic salt $Gd_2(SO_4)_3 \cdot 8H_2O$, while the temperature calibration above room temperature was based on the Curie-Weiss behavior of Gd_2O_3 and the known Curie temperature for Ni (631 K).

Figure 4 shows the bulk magnetization for $Fe_{3-x}Co_xSi$, σ (expressed in Bohr magnetons per formula unit) versus x for the $Fe_{3-x}Co_xSi$ alloys. The closed circles represent the saturation magnetization extrapolated to 0 K and infinite field, while the open circles represent the room-temperature magnetization extrapolated to infinite field. Data were obtained for the 14 samples with x ranging from 0 to 2.15. (Only the $x \leq 2.25$ samples possessed a second phase.) These measurements represent an extension of earlier work (Hines *et al.*[3]) for dilute Co concentrations

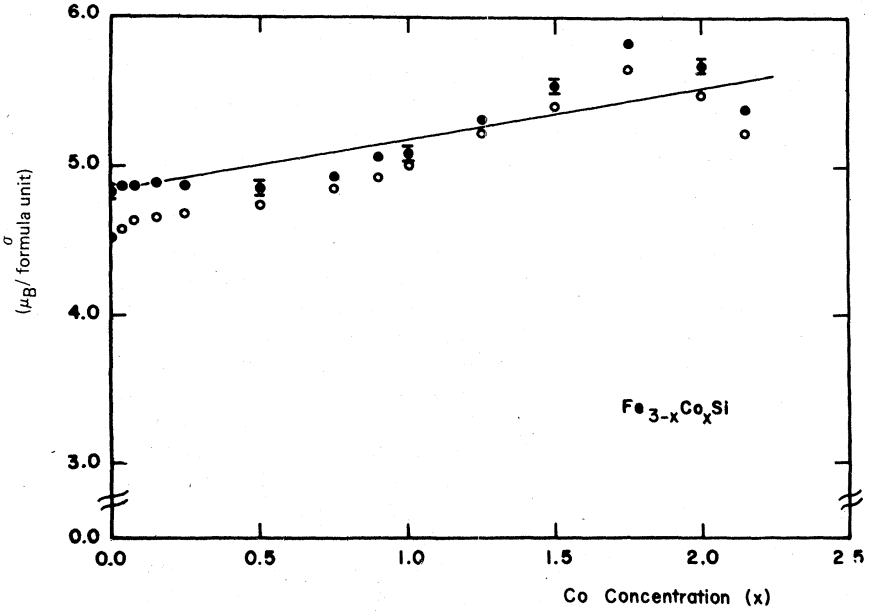

FIG. 4. Saturation magnetization σ (in μ_B per formula unit) vs Co concentration x, for $Fe_{3-x}Co_xSi$. Closed circles (0 K) and open circles (room temperature). Solid line: straight substitution of Co moments ($+1.70\mu_B$) for Fe moments ($+1.35\mu_B$) in the (A,C) sites.

($x \leq 0.25$). In the earlier work, moment assignments of $+2.20\mu_B$, $+1.35\mu_B$, and $-0.07\mu_B$ were made for Fe(B), Fe(A, C), and Si(D), respectively. Also in the earlier work, the saturation magnetization data for the $Fe_{3-x}Co_xSi$ alloys was fit reasonably well by a simple substitution model in which Co atoms with moments of $+1.70\mu_B$ replaced the Fe(A, C) atoms with moments of $+1.35\mu_B$ according to

$$\sigma = (+2.20) + (2-x)(+1.35) + (x)(+1.70) + (-0.07), \quad (1)$$

where σ is in μ_B per formula unit. The 1nn Fe(B) moments were assumed to be unchanged. Figure 4 shows an extension of this simple substitution model to the higher Co concentrations considered here (solid line). It can be seen that this simple substitution idea describes the overall increasing trend in the saturation magnetization as Co is added but does not follow the data in detail. The neutron-diffraction results presented below (Sec. II D) indicate that the Fe(B) and, consequently, Fe(A, C) moments vary with Co substitution which does not support the earlier assumption. Also, in Sec. III A we will describe how the detailed variation of σ vs x is completely consistent with the variation of the lattice constant with Co concentration x. An excellent fit to the lattice constant data is obtained by using a simple empirical relation consisting of a term containing the saturation magnetic moment (dashed line, Fig. 2). The empirical relation, an extension of Vegard' s law, has been successfully applied to several magnetic binary alloys by Shiga.[21] The individual variations of the Fe and Co moments will be described in Sec. II D concerning the neutron-diffraction measurements.

As Co is added to the Fe_3Si matrix, the magnetic-ordering temperature T_c increases. In particular, T_c increases from 839 K for Fe_3Si to 887 K for $Fe_{2.75}Co_{0.25}Si$. For $x \geq 0.50$, the magnetic-ordering temperatures are beyond the capabilities of the magnetometer oven.

D. Neutron diffraction

The neutron-diffraction measurements were performed at the Brookhaven National Laboratory and Rhode Island Nuclear Science Center Reactors, with an external magnetic field of 8 kOe applied along the scattering vector. The magnetization experiments described above indicate that the samples are essentially saturated at this field so that the magnetic scattering component is eliminated. All measurements were carried out at room temperature and the form factors were assumed to be the same as those for Fe_3Al and pure Co.

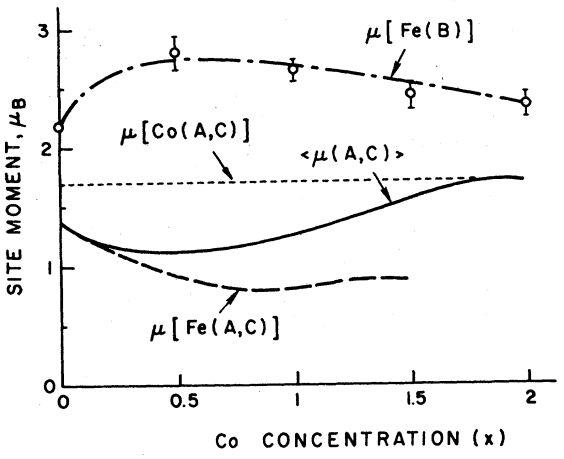

FIG. 5. Site moments μ (in μ_B) vs Co concentration x, for $Fe_{3-x}Co_xSi$. Open circles: experimental values for the Fe(B) moment from neutron diffraction (corrected to 0 K); dot-dashed curve: fit to data obtained from model; solid curve: average (A, C) site moment; dashed curve: Fe(A, C) moment; dotted curve: Co(A, C) moment ($+1.7\mu_B$).

Details of the neutron-diffraction pattern analysis are discussed elsewhere.[6]

The neutron-diffraction experiments have been carried out on four of the $Fe_{3-x}Co_xSi$ alloys yielding directly values for the room-temperature B site moment of $(+2.78 \pm 0.20)\mu_B$, $(+2.64 \pm 0.13)\mu_B$, $(+2.42 \pm 0.12)\mu_B$, and $(+2.37 \pm 0.12)\mu_B$ for $x = 0.50$, 1.00, 1.50, and 2.00, respectively. [These values were subsequently corrected to 0 K by a multiplication involving the appropriate ratio of magnetizations, $\sigma(0\text{ K})/\sigma(\text{RT})$.] The corrected moment values, along with the moment assignment of $+2.20\mu_B$ for Fe(B) in Fe_3Si ($x = 0$), are indicated in Fig. 5 by the open circles. The dot-dashed line represents a fit to the data that is obtained by employing a model based on 1nn configurations for the Fe(B) atoms (see Sec. III B).

The behavior of the average (A, C) site moment is obtained by subtracting the measured B site moment and D site moment [assuming Si(D) retains the value of $-0.07\mu_B$] from the total moment per formula unit obtained from the magnetization measurements (Fig. 4) and dividing by 2. The average (A, C) moment is indicated by the solid line in Fig. 5 and involves both Fe and Co atoms. Because of disorder, particularly for the higher Co concentrations, the B site moment will also involve a small number of Co atoms. We note that the average moment on the (A, C) sites becomes $+1.7\mu_B$ for $x = 2.00$. This is exactly the moment associated with the substituted Co atoms. Neglecting disorder, all of the Fe atoms in the (A, C) sites are replaced by Co atoms for the com-

position $x = 2.00$. It appears reasonable to assume that the substituted Co moment remains constant at $+1.7\mu_B$ throughout the entire range of composition as is the case in the binary $Fe_{1-c}Co_c$ system. Assuming a constant moment value of $+1.7\mu_B$ for $Co(A,C)$ (dotted line in Fig. 5), the moment values for $Fe(A,C)$ can be calculated from the average (A,C) site moment by a suitable subtraction. The behavior of the $Fe(A,C)$ moment is indicated by the dashed line in Fig. 5.

As indicated earlier, the neutron-diffraction results on the four alloys show no significant $(A,C) \rightleftharpoons B$ disorder for $x = 0.50$, 1.00, and 1.50, and 10% disorder for $x = 2.00$ (see Fig. 3). Such a disorder would indicate the presence of Co atoms in the B sites for $x = 2.00$.

E. Spin-echo NMR

Spin-echo NMR measurements of the internal hyperfine distributions were made on the various $Fe_{3-x}Co_xSi$ alloys at 1.3 K and with zero external magnetic field. The experimental apparatus, as well as the procedure of data taking, have been described in detail elsewhere.[22] No frequency correction has been used for the echo amplitude as the conclusions drawn from the NMR data are essentially independent of any such correction except where the spectral range is very large. In the present work, this only occurs for the Co resonance when $x \gtrsim 0.25$.

The internal field distributions observed in the $Fe_{3-x}Co_xSi$ alloys can be divided into two ranges. In the "low-frequency range," signals are observed from 20 to 70 MHz and are attributed to $Fe(A,C)$, $Fe(B)$, $Si(D)$, and, possibly, a small number of $Co(B)$ nuclei. The $Co(B)$ resonance is seen only for $x \geq 1.50$. Figures 6(a) and 6(b) show the spin-echo NMR spectra observed in the low-frequency range for the $Fe_{3-x}Co_xSi$ alloys with Co concentration ranging from $x = 0$ to 2.25. The lines due to $Fe(A,C)$, $Fe(B)$, and $Si(D)$ nuclei are indicated. For $x = 2.00$ and 2.25, a line occurs at approximately 36 MHz which has been associated with the $Co(B)$ nuclei.

In the "high-frequency range," signals are observed from 100 to 270 MHz and are attributed to $Co(A,C)$ nuclei. Figures 7(a) and 7(b) show the spin-echo NMR spectra of the ^{59}Co nuclei in the (A,C) sites observed in the high-frequency range for the $Fe_{3-x}Co_xSi$ alloys with x ranging from $x = 0.04$ to 2.25. The $Co(A,C)$, $Fe(A,C)$, $Fe(B)$, and $Si(D)$ resonances have already been reported for $Fe_{3-x}Co_xSi$ with low-Co concentration, $x \leq 0.25$, and our observations are consistent with this work.[4,5] Below, we will discuss in detail the spectral evolution for the various nuclei as a function of Co concentration.

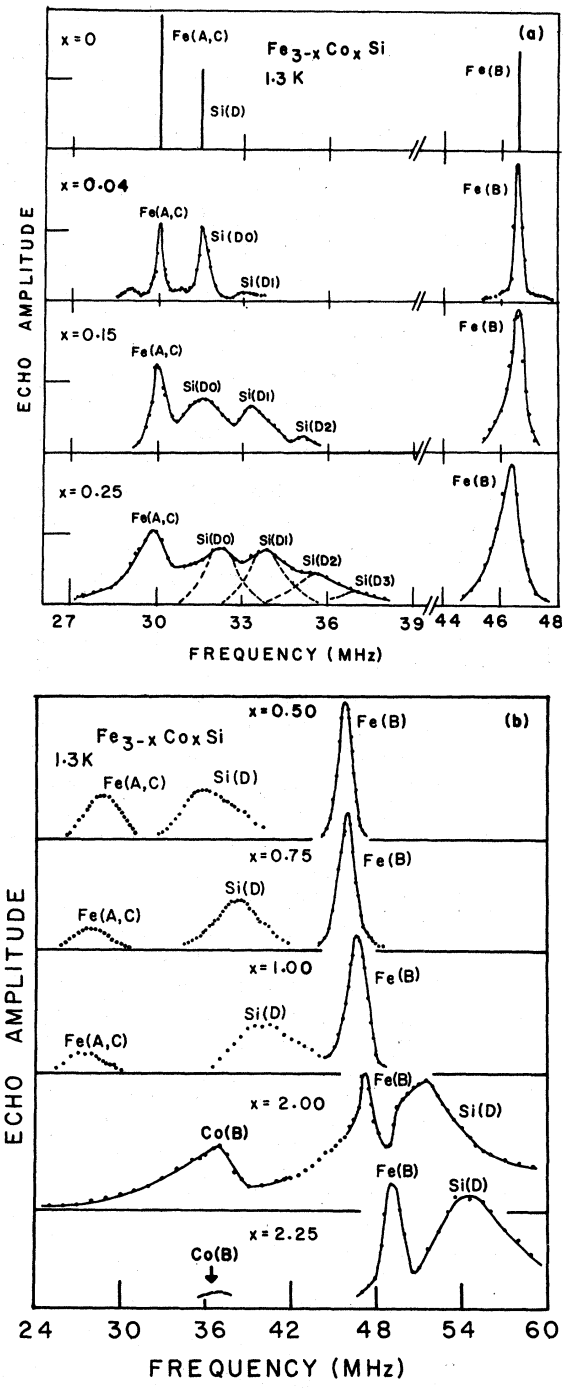

FIG. 6. Typical spin-echo NMR spectra observed in the "low-frequency range" (20–70 MHz) for the $Fe_{3-x}Co_xSi$ alloys: (a) $x = 0$–0.25, (b) $x = 0.50$–2.25. For $x = 2.00$ and 2.25, the line at approximately 36 MHz is associated with the $Co(B)$ nuclei.

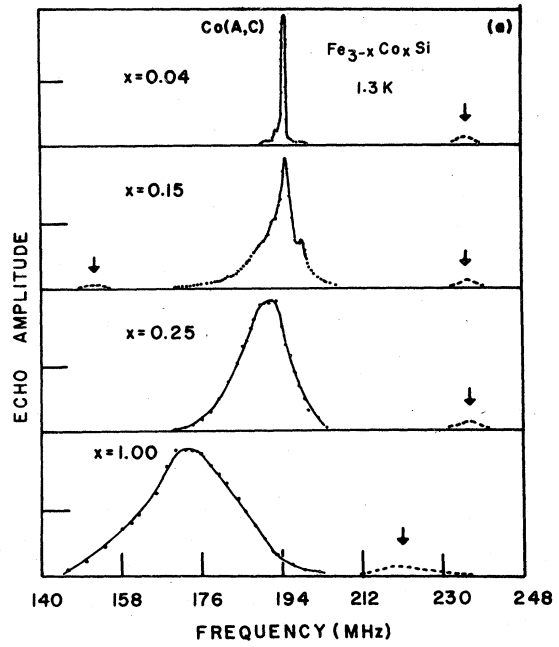

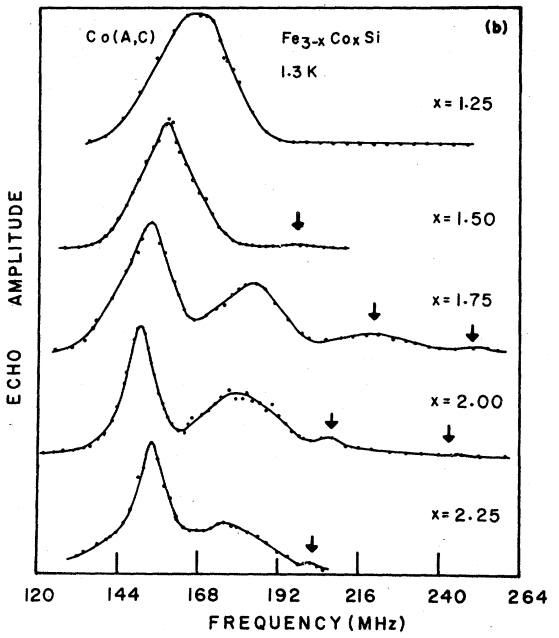

FIG. 7. Typical spin-echo NMR spectra observed in the "high-frequency range" (100–270 MHz) for the $Fe_{3-x}Co_xSi$ alloys: (a) $x=0.04$–1.00, (b) $x=1.25$–2.25. The arrows indicate the positions of weak Co(A,C) satellite lines which cannot be clearly shown on the scale chosen.

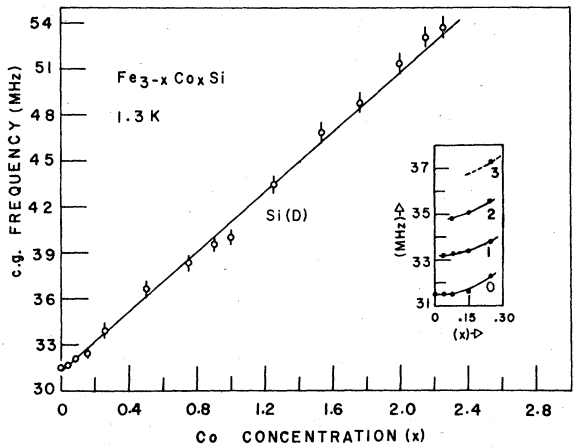

FIG. 8. Center of gravity of the Si(D) NMR spectral distribution (in MHz) vs Co concentration x, for $Fe_{3-x}Co_xSi$. Insert shows the position of the various Si(D) satellites vs x, visible only for $x \leq 0.25$. For insert, 0, 1, 2, and 3 indicate the number of Co atoms in the 1nn shell of Si(D).

1. Si(D) sites

As reported before, the resonance due to Si(D) appears at 31.5 MHz (37.2 kOe) in Fe_3Si ($x=0$).[4,5] The line is very sharp indicating a high degree of crystallographic order. As Co is added to Fe_3Si to form the $Fe_{3-x}Co_xSi$ alloys, the Co atoms enter the (A,C) sites which constitute the 1nn shell for Si(D) (see Table I). The presence of Co substitutions in the 4th, 7th, etc., neighbor shells is not considered to be important. As a result of 1nn Co substitutions, the Si(D) line exhibits distinct satellites on its high-frequency side [see Fig. 6(a)]. In particular, for $x=0.25$, three satellites are observed and correspond to Si with one Co atom in the 1nn shell [the Si$(D1)$ line], with two Co atoms in the 1nn shell [the Si$(D2)$ line], and three Co atoms in the 1nn shell [the Si$(D3)$ line]. The resolved Si lines are broadened due to presence of Co in more distant shells. The positions of all the Si(D) lines increase with x maintaining essentially the same separation of 1.6 MHz (1.9 kOe). Of particular interest for this system is whether the Co atoms enter all the (A,C) sites randomly or only the A or C sites. The intensities of the various Si(D) lines can be calculated for these two situations by using

$$P_n(m)=[n!/m!\,(n-m)!\,](c)^m(1-c)^{n-m}, \qquad (2)$$

where $P_n(m)$ is the probability of finding m impurities in any nn shell of n sites when the fractional impurity concentration is c. However, a good experimental determination of the Si(D) intensities for $Fe_{3-x}Co_xSi$ is only possible with the lower-Co concentrations ($x \leq 0.25$). For such low concentrations, the calculated intensities characteristic of the two substitution patterns described above are essentially the same making an experimental differentiation impossible. The observed intensities are not inconsistent with either pattern.

For $x \geq 0.50$ the satellite structure on the Si(D) is not visible [see Fig. 6(b)]. A broad Si(D) internal field distribution is observed at these compositions with the peak of the distribution shifting to higher frequencies with increasing x. Figure 8 shows the variation of the center of gravity of the Si(D) spectral distribution as a function of x for the $Fe_{3-x}Co_xSi$ alloys. The insert shows the variation of the distinct Si(D) satellites which are observed for $x \leq 0.25$.

2. Fe(B) sites

The sharp resonance due to Fe(B) appears at 46.6 MHz (337.7 kOe) in Fe_3Si ($x = 0$). Figure 9 shows the dependence of the Fe(B) internal field on x for the $Fe_{3-x}Co_xSi$ alloys (open circles). It can be seen that the Fe(B) internal field changes by less than ±2% over the entire composition range which is single phase. Contrary to expectations, the occurrence of Co in the 1nn shell does not produce any satellite structure or large shift of the Fe(B) line. Since the low-frequency NMR spectrum becomes increasingly complex for higher Co compositions, Mössbauer experiments were utilized to verify the assignment of the Fe lines. We note, however, that the Fe(B) moment changes substantially with x in this system (Fig. 5). The dashed line in Fig. 9 represents a fit to the data that is obtained by employing a model based on 1nn configurations for the Fe(B) atoms (see Sec. IIIC).

3. Fe(A,C) sites

The sharp resonance due to Fe(A,C) appears at 30.0 MHz (217.4 kOe) in Fe_3Si ($x = 0$). For very small additions of Co to Fe_3Si, a single satellite appears on each side of the main Fe(A,C) line. For $x = 0.04$, the satellites are located at 29.1 MHz (210.9 kOe) and 30.7 MHz (222.5 kOe) [see Fig. 6(a)] with their intensities in approximate agreement with the occurrence of a single Co atom in the 2nn and 3nn shells, respectively. For $x > 0.04$, the satellite structure on the Fe(A,C) resonance is not observed due to broadening of the main line as well as interference from the Si spectrum. Figure 10 shows the dependence of the Fe(A,C) internal field on x for $Fe_{3-x}Co_xSi$ (open circles). Since the Fe(A,C) atoms are being replaced by Co atoms, the Fe(A,C) resonance becomes weaker. The dashed line in Fig. 10 is a fit to the data that is obtained from the model (Sec. IIIC).

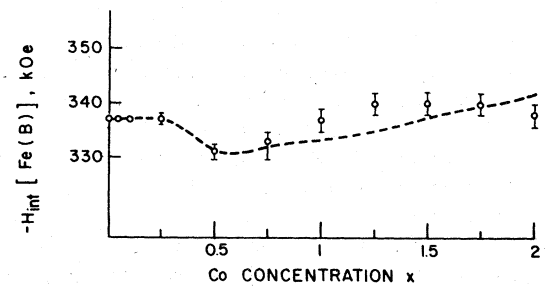

FIG. 9. Fe(B) internal hyperfine field, H_{int}[Fe(B)] (in kOe) vs Co concentration x, for $Fe_{3-x}Co_xSi$. Dashed curve: fit obtained from model.

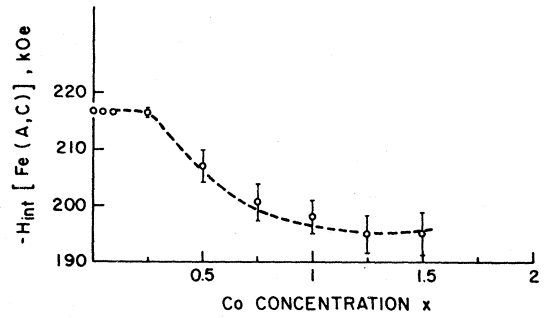

FIG. 10. Fe(A,C) internal hyperfine field, H_{int}[Fe(A,C)] (in kOe) vs Co concentration x, for $Fe_{3-x}Co_xSi$. Dashed curve: fit obtained from model.

4. Co(A,C) sites

For very small additions of Co to Fe_3Si, a signal is observed at 194.6 MHz (192.6 kOe), consistent with the early NMR work.[4,5] The evolution of the Co(A,C) NMR spectrum is illustrated in Figs. 7(a) and 7(b). For $x = 0.04$, two pairs of satellites are located symmetrically about the main Co(A,C) line; the inner (outer) pair having shifts of ±1.6 MHz (±3.8 MHz). The substitution of Co into the (A,C) sites results in 2nn, 3nn, and higher Co-Co interactions (see Table I). From a consideration of the satellite intensities, the low-frequency inner satellite is attributed to a single Co atom entering the 3nn shell, while the high-frequency inner satellite is attributed to a single Co atom entering the 2nn shell. Since the outer shifts are about twice the inner shifts, we are lead to attribute the low- (high-) frequency outer satellite to two Co atoms entering the 3nn (2nn) shell. The observed intensities of the outer satellites appeared somewhat larger than expected for a random distribution of Co into these shells. Figure 11 shows the variation of the main Co(A,C) internal field with x for $Fe_{3-x}Co_xSi$ (open circles), while the dashed line indicates the fit from the model.

Figure 7(a) shows arrows which indicate the positions of weak Co(A,C) satellite lines that cannot be clearly illustrated on the scale chosen. These satellites are attributed to a small amount

of $B \rightleftharpoons D$ disorder. Such a disorder will exchange Fe and Si atoms, and Co(A,C) will no longer have just four Fe and four Si as 1nn (see Table I). The arrow on the low-frequency side of the main Co(A,C) line (with four Fe and four Si as 1nn) indicates a satellite for the three Fe and five Si 1nn configuration, while the arrow on the high-frequency side indicates a satellite for the five Fe and three Si configuration. The intensities of these satellites are very small indicating a very small $B \rightleftharpoons D$ disorder for $x \leq 1.00$. The occurrence of satellites on the high-frequency side of the main Co(A,C) line for $x \geq 1.50$ [see arrows in Fig. 7(b)] is also attributed to $B \rightleftharpoons D$ disorder. As the frequency is increased from the main Co(A,C) line (with four Fe and four Si as 1nn), the satellites occur for the five Fe and three Si, six Fe, and two Si, etc., 1nn configurations. Assuming the disorder is random, an analysis of the intensities for the various satellites leads to estimates of the $B \rightleftharpoons D$ disorder. The $B \rightleftharpoons D$ disorder values for the various Co concentrations, x, in the $Fe_{3-x}Co_xSi$ alloys as determined from NMR are illustrated in Fig. 3.

In the low-frequency spectra of the $Fe_{3-x}Co_xSi$ alloys, an additional resonance, not attributable to Si(D), Fe(B), or Fe(A,C), is observed at approximately 36 MHz for $x \geq 2.00$ [see Fig. 6(b)]. This resonance has been attributed to small amounts of Co entering the B sites due to (A,C) $\rightleftharpoons B$ disorder. The large natural abundance of Co (100%) makes it possible to detect the small numbers of Co(B) nuclei with NMR.

III. DISCUSSION AND ANALYSIS

A. Structure, solubility, and degree of order

From x-ray measurements, we have established that, as the Co concentration is increased in the $Fe_{3-x}Co_xSi$ system, a single phase having the fcc DO_3-type structure is maintained (with some variation in lattice constant) up to $x = 2.15$. NMR has demonstrated that the Co atoms continue to substitute into the (A, C) sites for the higher concentrations studied in this work. Although the different methods (NMR, x-ray, and neutron diffraction) for determining the three types of disorder [$B \rightleftharpoons D$, (A, C) $\rightleftharpoons B$, and (A, C) $\rightleftharpoons D$] yield some variation in the disorder percentages, they all indicate that the system has very little disorder ($\lesssim 3\%$) for $x < 1.50$. For $x \geq 1.50$, the three types of disorder increase, reaching values ranging from 10% to 16% for the $x = 2.00$ composition. All of the samples with $x \geq 2.25$ possessed a second phase.

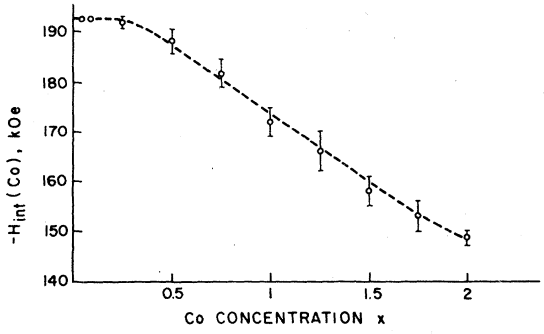

FIG. 11. Co(A,C) internal hyperfine field, H_{int}[Co(A,C)] (in kOe) vs Co concentration x, for $Fe_{3-x}Co_xSi$. Dashed curve: fit obtained from model.

The $Fe_{3-x}Co_xSi$ alloys are ferromagnetic for $0 \leq x \leq 2.15$. Shiga[21] has found that a simple empirical relation between the lattice constant and the magnetic moment holds for numerous binary systems involving $3d$ transition metals which form solid solutions over considerable ranges of composition. Since the same $3d$ electrons which are responsible for the magnetic moments of transition elements are also involved in the cohesion of transition metals, a correlation between the magnetic moment and the atomic distance is expected. Shiga's empirical relation, which is an extension of Vegard's law to include magnetic properties and their influences, is written

$$a(c) = a_A(1-c) + a_B(c) + C\langle\mu\rangle, \tag{3}$$

where $a(c)$ is the lattice constant of the binary solid solution $A_{1-c}B_c$, a_A, a_B, and C are adjustable parameters and $\langle\mu\rangle$ is the "average magnitude of the atomic moments." As indicated above, this simple relationship works well for several binary systems including $Fe_{1-c}Co_c$. For nonmagnetic alloys, $\langle\mu\rangle = 0$ and Eq. (3) becomes Vegard's law. For simple ferromagnetic alloys, $\langle\mu\rangle$ may be equated with the saturation magnetization in Bohr magnetons per formula unit.

Following Shiga's ideas, we can construct an equivalent empirical relation for our ternary $Fe_{3-x}Co_xSi_x$ system. We write

$$a(x) = a_{Fe}(\tfrac{3}{4} - \tfrac{1}{4}x) + a_{Co}(\tfrac{1}{4}x) + a_{Si}(\tfrac{1}{4}) + C\langle\mu\rangle, \tag{4a}$$

where, in Shiga's description, the parameters a_{Fe}, a_{Co}, and a_{Si} can be related to the atomic sizes of the respective elements by a factor which depends on the lattice structure. By simple algebraic manipulation, we can combine the parameters and put Eq. (4a) in a more suitable form for fitting our lattice constant data. We rewrite

$$a(x) = a_1(1 - \tfrac{1}{4}x) + a_2(\tfrac{1}{4}x) + C\langle\mu\rangle, \tag{4b}$$

where $a_1 = a_{Fe} + \frac{1}{4}(a_{Si} - a_{Fe})$ and $a_2 = a_{Co} + \frac{1}{4}(a_{Si} - a_{Fe})$. Values for the parameters a_1, a_2, and C were obtained by fitting Eq. (4b) to the room-temperature lattice constant data of Fig. 2 for three Co

concentrations ($x = 0$, 1.00, 1.50). The corresponding moment values $\langle\mu\rangle$ were taken from Fig. 4. It was found that, with the parameters obtained, Eq. (4b) described the rest of the lattice constant data extremely well over the range of composition $0 \leq x \leq 2.00$. This is illustrated by the dashed curve in Fig. 2. The values for the parameters were $a_1 = 5.4796$ Å, $a_2 = 5.3848$ Å, and $C = 0.0360$ Å/μ_B. We note that the magnetic parameter, $C = 0.0360$ Å/μ_B is typical of such values found in the magnetic binary systems (e.g., $C = 0.0324$ Å/μ_B for $Fe_{1-c}Co_c$). Note that, with the empirical form above, it is not possible to uniquely determine the original paramters a_{Fe}, a_{Co}, and a_{Si}.

B. Magnetic-moment formation

In order to understand the origin and behavior of the internal hyperfine fields in $Fe_{3-x}Co_xSi$ (see Sec. III C), it is important to know the local magnetic moment on each site and not just the total moment per formula unit as determined from saturation magnetization measurements alone. As discussed in Sec. II D, such information has been obtained from a combination of the neutron-diffraction and magnetization results and is presented in Fig. 5. For increasing Co concentration x, the Fe(B) moment increases quickly from a value of $+2.20\mu_B$ for $x = 0.50$, and then decreases slowly, becoming $+2.42\ \mu_B$ for $x = 2.00$. There is evidence to indicate that the Co atoms maintain a constant moment of $+1.7\ \mu_B$ throughout the entire range of composition as they selectively replace the Fe(A, C) atoms. Finally, the average Fe(A, C) moment decreases from a value of $+1.35\mu_B$ for $x = 0$ and passes through a minimum at $x \approx 0.50$.

Due to the structural similarity, it is tempting to compare the magnetic behavior we observe for the $Fe_{3-x}Co_xSi$ alloys with the binary $Fe_{1-c}Co_c$ system. $Fe_{1-c}Co_c$ forms a continuous range of solid solutions with the bcc structure from $c = 0$ to 0.75. Additionally, this system exhibits an order-disorder transition over a large portion of its composition range such that the equiatomic alloy ($c = 0.50$) possesses the CsCl-type structure.

Bardos[23] has measured the saturation magnetization (magnetic moment per formula unit) for $Fe_{1-c}Co_c$ as a function of Co concentration ($c = 0$–0.70) and degree of order. Neutron-diffraction measurements have been performed by Collins and Forsyth[24] for $c = 0.30$, 0.50, and 0.70. An analysis of the magnetization and neutron-diffraction results leads to the conclusion that the moment on the Co atoms remains essentially constant ($+1.8\mu_B$) throughout the entire range of composition. In addition, the magnetic moment on an Fe atom is determined by the number of Co 1nn. In particular, the 1nn shell for an Fe (or Co) atom has eight sites in this bcc-like structure. As the number of Co 1nn varies from zero to eight, the average Fe moment increases from $+2.20\mu_B$ to $+3.05\mu_B$.

For the $Fe_{3-x}Co_xSi$ system, the Fe(B) atoms also have a 1nn shell of eight sites in a cubic arrangement [the (A,C) sites]. As the Co concentration is increased from $x = 0$ to 2.00, Fe in the (A,C) sites is replaced by Co. The number of Co atoms in the 1nn shell of an Fe(B) atom can vary from zero to eight as it does in $Fe_{1-c}Co_c$. Our results suggest, that Co substitutes into $Fe_{3-x}Co_xSi$ over the range from $x = 0$ to 2.00 with a constant moment of $+1.7\mu_B$ which is consistent with the $Fe_{1-c}Co_c$ behavior. However, the Fe(B) moment does not increase quite as much with its number of Co 1nn as the Fe moments in $Fe_{1-c}Co_c$. Also, the B site moment actually shows a small decrease for $x > 0.50$. Since a model describing the dependence of the Fe(A,C) moment solely on its 1nn configurations was very successful in analyzing the internal field behavior for the $Fe_{1-x}Si_x$, $Fe_{3-x}V_xSi$, and $Fe_{3-x}Mn_xSi$ systems [in which Si, V, and Mn replace Fe(B)],[1] it is tempting to construct a model based solely on the 1nn configurations for the Fe(B) moment in $Fe_{3-x}Co_xSi$ [in which Co replaces Fe(A,C)]. The best insight for such a model comes from the direct measurement of the Fe(B) moment from neutron diffraction. It must be kept in mind that such a measurement actually represents an average value for the Fe(B) site moment. For a given Co concentration, there will be some distribution of 1nn configurations and the probability of occurrence for a given configuration can be calculated by Eq. (2).

Figure 12 illustrates the model we present in this work which describes the dependence of a single Fe(B) moment on the number of Co atoms in its 1nn shell. The addition of a single Co atom

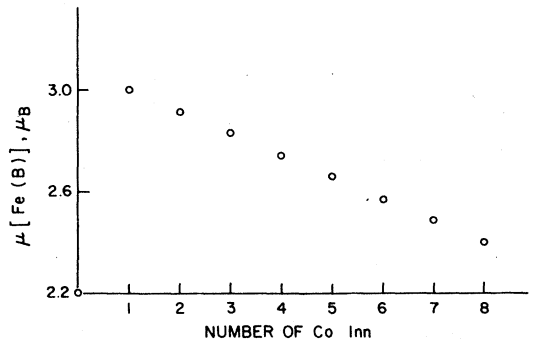

FIG. 12. Moment of a single Fe(B) atom, μ[Fe(B)] (in μ_B) vs number of Co 1nn as proposed by model.

into the 1nn shell of a Fe(B) atom increases its moment from $+2.20\mu_B$ to $+3.00\mu_B$. A further increase in the number of Co 1nn produces a gradual decrease in the Fe(B) moment until a value of $+2.40\mu_B$ is obtained for eight Co 1nn. Hence the (average) Fe(B) moment, as observed in the neutron experiments, is given by

$$\langle \mu[\mathrm{Fe}(B)] \rangle = \sum_{i=0}^{8} P_i \mu_i , \tag{5}$$

where P_i is the probability of a single Fe(B) atom having i 1nn of Co [Eq. (2)] and μ_i is the moment of that atom as dictated by the model (Fig. 12). The dot-dashed line in Fig. 5 was calculated from Eq. (5) and provides an excellent fit to the experimental data.

C. Internal field behavior

For systems involving transition metals, the internal hyperfine field at a particular nucleus H_{int} is assumed to arise from three contributions: (i) a core polarization due to the exchange interaction between the on-sight moment of the d electrons and the inner s shells, H_{cp}, (ii) a spin polarization of the conduction s electrons due to the on-site moment of the atom itself, H_s, and (iii) an overall (transferred) conduction-electron-spin polarization due to the moments in neighboring shells, H_{sp}. Hence, we can write

$$H_{\mathrm{int}} = H_{\mathrm{cp}} + H_s + H_{\mathrm{sp}} . \tag{6}$$

In general, the first two terms are proportional to the on-site moment, while the third term is usually expressed as a sum of terms involving the neighboring moments. As a first approximation, we will assume that the transferred spin polarization at a nuclear site arises only from the moments in its 1nn shell and is given by

$$H_{\mathrm{sp}} = A_{4s} n p \langle \mu \rangle_{1\mathrm{nn}} , \tag{7}$$

where A_{4s} is the appropriate hyperfine coupling constant, n is the number of 4s electrons involved in the hyperfine coupling, p is the exchange polarization of the 4s electrons by the 3d moments, and $\langle \mu \rangle_{1\mathrm{nn}}$ is the average moment per atom in the 1nn shell. Such an approach has proved very successful in describing the internal field behavior for the $Fe_{3-x}Si_x$, $Fe_{3-x}V_xSi$ and $Fe_{3-x}Mn_xSi$ systems.[1] We will use the atomic hyperfine coupling constants calculated by Campbell.[25] As pointed out by Campbell, the A_{4s} values are deduced by an interpolation of the atomic hyperfine coupling constants between the alkali and noble metals and, although the absolute values are not expected to describe accurately the coupling in metals, the relative values of A_{4s} for elements close to one another in the periodic table are expected to be reasonably correct.

In the following, we will be concerned mostly with the main Co resonance. Figure 11 shows the concentration dependence of the Co internal field in $Fe_{3-x}Co_xSi$. The principal contributions to the Co internal field, $H_{\mathrm{int}}[\mathrm{Co}A,C)]$, are described by Eqs. (6) and (7). The polarization terms $(H_{\mathrm{cp}}[\mathrm{Co}(A,C)] + H_s[\mathrm{Co}(A,C)])$ are due to the on-site Co 3d moment, while $H_{\mathrm{sp}}[\mathrm{Co}(A,C)]$ is transferred from the surrounding Fe(B) moments. Co replaces Fe in the (A,C) sites with four Fe(B) and four Si(D) 1nn in the ordered atomic state. By assuming that the Co moment remains constant ($+1.7\mu_B$) throughout the entire range of composition and, hence, that the on-site polarization terms $(H_{\mathrm{cp}}[\mathrm{Co}(A,C)] + H_s[\mathrm{Co}(A,C)]$ do not change, it follows that the change in $H_{\mathrm{int}}[\mathrm{Co}(A,C)]$ with increasing concentration is due mainly to the change in the transferred spin polarization of the Co 4s electrons by $\langle \mu[\mathrm{Fe}(B)] \rangle_{1\mathrm{nn}}$. By considering the Fe($B$) moment dependence on the number of Co 1nn as described by the model proposed in Sec. III B (see Fig. 12) a very good fit of the concentration dependence for $H_{\mathrm{int}}[\mathrm{Co}(A,C)]$ is obtained by taking $A_{4s}(\mathrm{Co}) = 2.05 \times 10^6$ Oe/(s electron) and $np = -71.51 \times 10^{-3}$ (s electron)/μ_B in Eq. (7) above (dashed line in Fig. 11). This results in a calculated value for the onsite polarization terms of $(H_{\mathrm{cp}}[\mathrm{Co}(A,C)] + H_s[\mathrm{Co}(A,C)]) = +27$ kOe. The very small and positive value for the hyperfine-field contributions corresponding to the on-site moment of $+1.7\ \mu_B$ (or $+15.9$ kOe/μ_B) is contrasted with the large negative fields derived for Fe (-205 kOe) and Mn (-192 kOe) and indicates a relative large positive contribution from $H_s[\mathrm{Co}(A,C)]$.

The value of +27 kOe obtained above for the on-site moment polarization contributions seems quite reasonable in the light of other systems in which Co atoms are introduced into environments where the 1nn atoms do not possess localized moments. This is exactly the case for the Heusler alloys of the type Co_2XY, where X = Ti, Zr, Hf, V, and Nb, and Y = Sn, Al, and Cr. The magnetic moment in these materials is confined to the Co atoms with values ranging from $+0.3\ \mu_B$ to $+1.0\ \mu_B$, The 4 X and 4 Y atoms which surround the Co atoms possess essentially no magnetic moment and, hence, the only contribution to the Co internal field arises from the on-site contributions. NMR studies in Co_2TiSn, for which $\mu(\mathrm{Co}) = +1.03\mu_B$, gave a value of +21.2 kOe for the Co internal field at 77 K.[26] More recent internal field measurements in other Co-based Heusler alloys also demonstrated Co fields which were positive and of comparable magnitude to the value calculated in this work.[27]

Moreover, it should be mentioned that when the A_{4s}(Co) and np parameters given above are used with Eq. (7), a value of $H_{sp}[\mathrm{Co}(A,C)] = -220$ kOe is calculated at the Co nucleus for very dilute Co concentrations. If one extra Fe atom is added to the 1nn shell of a Co atom (and having $\mu[\mathrm{Fe}(B)] = +3.0\mu_B$), $H_{sp}[\mathrm{Co}(A,C)]$ would be increased in magnitude by about 55 kOe resulting in a Co resonance corresponding to $H_{int}[\mathrm{Co}(A,C)] = -248$ kOe (251 MHz). Furthermore, removing an Fe atom from the 1nn shell of a Co atom would decrease $H_{sp}[\mathrm{Co}(A,C)]$ by 55 kOe in magnitude resulting in a Co resonance corresponding to $H_{int}[\mathrm{Co}(A,C)] = -138$ kOe (139 MHz). Previously, we have noted the occurrence of very weak satellite lines (152 and 236 MHz) located symmetrically below and above the main Co line (194.6 MHz). The small amount of disorder ($\lesssim 3\%$) for low-Co concentrations is sufficient to create situation in which a Co atom would have either 3 Fe(B) or 5 Fe(B) in its 1nn shell giving rise to the satellite lines. This assignment for the satellite lines has been confirmed by observing the Co resonance in off-stoichiometric alloys.

The internal fields for the Fe(B) and Fe(A,C) nuclei can also be described by the methods above. Figure 9 illustrates the concentration dependence of the Fe(B) internal field. It can be seen that the field changes by less than ±2% over the composition range $0 \leq x \leq 2.00$. In order to calculate the on-site contributions ($H_{cp}[\mathrm{Fe}(B)] + H_s[\mathrm{Fe}(B)]$), to the internal field, we take the value -93.18 kOe/μ_B which was found for the Fe atoms in $Fe_{1-x}Si_x$, $Fe_{3-x}V_xSi$, and $Fe_{3-x}Mn_xSi$ (see ref.[1]). The Fe(B) moment is dictated by the number of Co 1nn as described by the model (Fig. 12). The polarization transferred from the 1nn shell, $H_{sp}[\mathrm{Fe}(B)]$, is a combination of the contributions from both the Co and Fe in the (A,C) sites for which the respective polarization factors of $np = -39\times10^{-3}$ (s electron)/μ_B and $np = -25\times10^{-3}$ (s electron)/μ_B have been assigned. The hyperfine coupling constant for the Fe atoms is taken to be $A_{4s}(\mathrm{Fe}) = 1.78\times10^6$ Oe/(s electron). Using Eqs. (6) and (7) above, a good fit of the experimental data is obtained (dashed line in Fig. 9).

Fig. 10 shows the concentration dependence of the internal field in $Fe_{3-x}Co_xSi$. Again, an excellent fit of the Fe(A,C) internal field (dashed line in Fig. 10) of the experimental data is obtained by calculating: (a) the onsite contribution from -93.18 kOe/μ_B and the Fe(A,C) moment assignment at various Co concentrations (Fig. 5) and (b) the transferred contribution from the surrounding Fe(B) moments with a polarization factor of $np = -47\times10^{-3}$ (s electron)/μ_B.

In general, the model proposed, which utilizes the short-range interaction approach and involves the 1nn configurations for the Fe(B) atoms, provides an excellent description of the magnetic-moment and internal field behavior for the Co(A,C), Fe(B), and Fe(A,C) sites.

IV. SUMMARY AND CONCLUSIONS

This work concerned a detailed NMR, magnetization, x-ray, and neutron-diffraction study of the $Fe_{3-x}Co_xSi$ system over the entire range of composition ($0 \leq x \leq 3.00$) in order to: (i) determine the crystallographic and magnetic structure, (ii) further explore the nature and concentration limits of the site selectivity, and (iii) determine the dependences of the Fe, Co, and Si magnetic moments and internal hyperfine fields on the local environment. As indicated earlier, systems involving transition metal substitutions into the Fe_3Si lattice have proved ideal for such studies[1-17] and a local environment model has previously been developed for such substitutions into the B sites.[1] Below, we list the conclusions of the present work.

(i) As the Co concentration is increased in the $Fe_{3-x}Co_xSi$ system, a single phase having the fcc DO_3-type structure is maintained (with some variation in lattice constant) up to $x = 2.15$.

(ii) The Co atoms selectively enter the (A,C) sites for the larger concentrations studied in this work ($0 \leq x \leq 2.00$) with a high degree of order (disorder values $\lesssim 3\%$ for $x < 1.50$).

(iii) The $Fe_{3-x}Co_xSi$ alloys are ferromagnetic for $0 \leq x \leq 2.15$. The variation in lattice constant with Co concentration correlates well with the magnetization and can be described by a simple empirical relation which is an extension of Vegard's law.

(iv) Neutron-diffraction results indicate a variation in the Fe(B) and, consequently, the Fe(A,C) moments with Co concentration. However, there is evidence to indicate that the moment on the substituted Co atom is well localized and remains constant at $+1.7\mu_B$ throughout the range $0 \leq x \leq 2.15$.

(v) The variation of the internal hyperfine field with Co concentration at all sites [Fe(A,C), Fe(B), Co(A,C), and Si(D)] has been studied by spin-echo NMR. A model which describes the dependence of a single Fe(B) moment on the number of Co atoms in its 1nn shell is introduced that successfully explains the internal field behavior. In this model, the addition of one Co atom to the 1nn shell of a Fe(B) atom increases its moment from $+2.20\mu_B$ to $+3.00\mu_B$. A further increase in the number of Co 1nn gradually decreases the Fe(B) moment until a value of $+2.40\mu_B$ is obtained for eight Co 1nn.

TABLE II. Internal field parameters for $Fe_{3-x}Co_xSi$.

Nucleus	1nn configuration	$(H_{cp}+H_s)/\mu$ (k0e/μ_B)	A_{4s} (M0e/s electron)	np [10^{-3}(s electron/μ_B]
Co(A,C)	4 Fe(B), 4 Si(D)	+15.9	2.05	−71.5
Fe(B)	8 [Fe(A,C) + Co(A,C)]	−93.18	1.78	−25(Fe), −39(Co)
Fe(A,C)	4 Fe(B), 4 Si(D)	−93.18	1.78	−47

The Fe(A,C), Fe(B), and Co(A,C) hyperfine-field values are separated into contributions resulting from the on-site moment and that transferred from neighboring moments. Table II provides a summary of the parameters used to calculate the internal hyperfine-field contributions for the various nuclei according to the model. Column 1 lists the nuclei and their sites while column 2 lists the 1nn configurations. Column 3 lists the ratios of the on-site internal field contributions to the on-site moments. Columns 4 and 5 list the hyperfine-coupling constants and polarization factors used in calculating the internal field contribution transferred from the 1nn moments.

Currently, a similar study is in progress for the $Fe_{3-x}Ni_xSi$ system. Like Co, Ni is found to substitute into the (A,C) sites over a considerable range of composition ($0 \leq x \leq 1.00$). Preliminary results indicate that a local environment model, consistent with the one proposed here, provides an excellent description of the magnetic-moment and internal field behavior.

ACKNOWLEDGMENTS

The authors wish to thank A. H. Menotti for her assistance with the magnetization measurements at the University of Connecticut, and C. F. Majkrzak and C. K. Saw for their assistance with the neutron-diffraction measurements at the Rhode Island Nuclear Science Center. We are grateful to A. Corbeil for his help in the preparation of samples. This work was supported in part by the University of Connecticut Research Foundation.

*Present address: Department of Physics, Virginia Commonwealth University, Richmond, Virginia 23284.
†Present address: Ferrofluidics Corp. Burlington, Massachusetts 01803.

[1]V. Niculescu, K. Raj, J. I. Budnick, T. J. Burch, W. A. Hines, and A. H. Menotti, Phys. Rev. B 14, 4160 (1976).
[2]R. L. Bergner, V. U. S. Rao, and S. G. Sankar, AIP Conf. Proc. 29, 325 (1976).
[3]W. A. Hines, A. H. Menotti, J. I. Budnick, T. J. Burch, T. Litrenta, V. Niculescu, and K. Raj, Phys. Rev. B 13, 4060 (1976).
[4]T. J. Burch, T. Litrenta, and J. I. Budnick, Phys. Rev. Lett. 33, 421 (1974).
[5]T. Litrenta, Ph.D. thesis (Fordham University, 1975) (unpublished).
[6]S. Pickart, T. Litrenta, T. J. Burch, and J. I. Budnick, Phys. Lett. A 53, 321 (1975).
[7]S. Yoon and J. G. Booth, Phys. Lett. A 48, 381 (1974).
[8]C. Blaauw, G. R. Mackay, and W. Leiper, Solid State Commun. 18, 729 (1976).
[9]A. C. Switendick, Bull. Am. Phys. Soc. 21, 441 (1976).
[10]A. C. Switendick, Solid State Commun. 19, 511 (1976).
[11]V. Niculescu, K. Raj, T. J. Burch, and J. I. Budnick, Phys. Rev. B 13, 3167 (1976).
[12]J. G. Booth, J. E. Clark, J. D. Ellis, P. J. Webster, and S. Yoon, Proceedings of the International Conference on Magnetism, Moscow, 1973 (unpublished), Vol. IV, p. 577.
[13]K. Raj, V. Niculescu, J. I. Budnick, and S. Skalski, AIP Conf. Proc. 29, 348 (1976).
[14]K. Raj, V. Niculescu, T. J. Burch, J. I. Budnick, and R. B. Frankel, AIP Conf. Proc. 34, 28 (1977).
[15]V. Niculescu, T. J. Burch, K. Raj, and J. I. Budnick, J. Magn. Magn. Mater. 5, 60 (1977).
[16]V. Niculescu, T. Litrenta, K. Raj, T. J. Burch, and J. I. Budnick, J. Phys. Soc. Jpn. 42, 1538 (1977).
[17]J. I. Budnick *et al.*, Bull. Am. Phys. Soc. 20, 457 (1975); 20, 586 (1975); 20, 586 (1975); 20, 587 (1975); 21, 441 (1976); 22, 26 (1977); 22, 116 (1977); 22, 458 (1977); 23, 227 (1978).
[18]See Refs. 5, 6, and 18 in Hines *et al.*, Phys. Rev. B 13, 4060 (1976).
[19]See Refs. 7–11 and 18 in Hines *et al.*, Phys. Rev. B 13, 4060 (1976).
[20]S. Foner, Rev. Sci. Instrum. 30, 548 (1959).
[21]M. Shiga, AIP Conf. Proc. 18, 463 (1974).
[22]J. I. Budnick and S. Skalski, in *Hyperfine Interactions*, edited by A. J. Freeman and R. Frankel (Academic, New York, 1967), p. 724.
[23]D. I. Bardos, J. Appl. Phys. 40, 1371 (1969).
[24]M. F. Collins and J. B. Forsyth, Philos. Mag. 8, 401 (1968).
[25]I. A. Campbell, J. Phys. C 2, 1338 (1969).
[26]K. Endo, A. Shinogi, and I. Vince, J. Phys. Soc. Jpn. 40, 674 (1976).
[27]R. Vijayaraghavan, A. K. Grover, L. C. Gupta, V. Nagarajan, J. Itok, K. Shimizu, and H. Mizutani, J. Phys. Soc. Jpn. 42, 1779 (1977).